Applied Catalysis B: Environmental 166–167 (2015) 132–144

Contents lists available at ScienceDirect

Applied Catalysis B: Environmental

journal homepage: www.elsevier.com/locate/apcatb

Continuous regime of chemical-looping combustion (CLC) and chemical-looping with oxygen uncoupling (CLOU) reactivity of CuO oxygen carriers

Zhiquan Zhou, Lu Han, Oscar Nordness, George M. Bollas*

Department of Chemical & Biomolecular Engineering, University of Connecticut, 191 Auditorium Road, Unit 3222, Storrs, CT 06269-3222, USA

ARTICLE INFO

Article history:
Received 17 August 2014
Received in revised form 24 October 2014
Accepted 24 October 2014
Available online 15 November 2014

Keywords:
Chemical-looping
Chemical-looping with oxygen uncoupling
Cu catalyzed reactions
CuO reduction

ABSTRACT

Chemical-looping with CuO and CH_4 presents an interesting reaction system, in which CuO participates in heterogeneous reduction reactions with the gaseous fuel, as well as oxygen uncoupling and catalytic reactions. Therefore, there exists a temperature dependent competition between the processes typically termed as chemical-looping combustion (CLC) and chemical-looping with oxygen uncoupling (CLOU). The objective of this work is to carry out an assessment of the rates of all the relevant reactions involved at various temperatures and thus to show a continuous regime, where the CLC reactions domination proceeds to CuO oxygen uncoupling dominance, as temperature increases. The possible reactions occurring in CuO-based chemical-looping include heterogeneous reactions with Cu oxides, CuO oxygen uncoupling and Cu-catalyzed reactions. The significance of each individual reaction and the corresponding kinetic parameters are experimentally examined in a bench-scale fixed-bed, alternating-flow chemical-looping reactor at conditions relevant to both CLC and CLOU. *In situ* XRD characterization is used to determine the phases in which Cu exists during reduction and oxidation and possible interactions with the SiO_2 oxygen carrier support. A kinetic scheme is proposed, applicable to the entire regime of CLC and CLOU, which is validated with in-house experiments and experimental data from the literature, at conditions where heterogeneous reduction, oxygen uncoupling, Cu-catalyzed, and gas phase oxidation reactions present significant contributions.

1. Introduction

Chemical-looping combustion (CLC) enables the concentration of high purity CO_2 from fossil fuels combustion at a small energy penalty. This concept is achieved through the pairing of two reactors – a Reducer and an Oxidizer utilizing a metal oxide as the oxygen transport agent. A modification of the CLC process, known as chemical-looping with oxygen uncoupling (CLOU) was proposed by Mattission et al. [1]. The CLOU process employs certain metal oxides as oxygen carriers (OCs), taking advantage of their exothermic and spontaneous splitting at high temperatures, resulting in an overall thermodynamically favorable process for the transport of oxygen from air to a fuel oxidation reactor. The main benefit of CLOU, operating with solid fuels, is its ability to overcome the slow solid–solid reduction and solid gasification reactions of CLC, thus allowing for the combustion of fuels like coal and biomass [2].

The CLOU process requires an OC to uncouple at high temperatures and generate gaseous oxygen, which depends on the metal oxide thermodynamic and kinetic properties. Several metal oxide systems have been identified and used for CLOU, including CuO/Cu_2O, Mn_2O_3/Mn_3O_4, Co_3O_4/CoO, combined oxides and perovskites [3], among which, Cu-based OCs are mostly studied and widely used [4]. Due to their high reaction rates and high oxygen carrying capacity, Cu-based OCs have been investigated in thermogravimetric analyzers (TGA) [5–11], fixed-beds [12,13], semi-batch fluidized beds [14–17] and interconnected fluidized beds with continuous OC circulation [18,19] for both CLC and CLOU applications. However, the relatively low melting temperature of Cu (1273 K) presents a challenge. Accumulative thermal sintering and agglomeration phenomena may occur when Cu is used as the OC in the harsh CLC environment [20]. To address this issue, several Cu OC supports were investigated in the literature, identifying that Cu/SiO_2 exhibits negligible performance change caused by thermal sintering [12]. Therefore, SiO_2 supported CuO [7,9,12,21–23] has been extensively studied and proposed as a promising CLC/CLOU material. Due to its advantages and extensive use, CuO/SiO_2 was chosen as the oxygen carrier for this study.

* Corresponding author. Tel.: +1 8604864602.
E-mail address: george.bollas@uconn.edu (G.M. Bollas).

http://dx.doi.org/10.1016/j.apcatb.2014.10.067
0926-3373/

Notation (model equations can be found in the Supporting Information)

a_0	initial specific surface area of the oxygen carrier (m^2/kg OC)
C_i	concentration of gas species i (mol/m^3)
$C_{p,f}$	heat capacity of the gas mixture of the fluid phase (J/mol K)
$C_{p,s}$	heat capacity of solid (J/mol K)
C_T	total gas concentration in fluid phase (mol/m^3)
C_{Cu}	Cu concentration (kg Cu/kg OC)
C'_{CuO}	initial CuO concentration (kg Cu/kg OC)
D_t	diameter of the reactor tube (m)
$D_{ax,i}$	axial dispersion coefficient of species i (m^2/s)
Ea_j	activation energy for reaction j (kJ/mol)
F_i	molar flow rate of gas species i (mol/s)
F_T	total molar flow rate of gas species (mol/s)
i	gas phase species (CH_4, H_2, H_2O, CO, CO_2, O_2, Ar, N_2)
j	chemical reaction
k_j	rate constant for reaction j
$k_{1-8,0}$	pre-exponential factor for rate constant k_1-k_8 (m/s)
$k_{9,0}$	pre-exponential factor for rate constant k_9 (kmol/m^2 s bar)
$k_{10,0}$	pre-exponential factor for rate constant k_{10} (kmol/kg s bar^4)
$k_{11,0}$	pre-exponential factor for rate constant k_{11} (kmol/kg s bar^2)
$k_{12-13,0}$	pre-exponential factor for rate constant k_{12-13}(kmol/kg s bar)
$k_{14,0}$	pre-exponential factor for rate constant k_{14} (kmol/kg s $bar^{1.5}$)
K_{10}	equilibrium constant for dry reforming (bar^2)
K_{11}	equilibrium constant for water gas shift (–)
K_{CO}	CO adsorption term for R14 (bar^{-1})
K_{H_2}	H_2 adsorption term for R13 (bar^{-1})
$K_{O_2,13}$	O_2 adsorption term for R13 (bar^{-1})
$K_{O_2,14}$	O_2 adsorption term for R14 (bar^{-1})
n	Avrami exponent for the Avrami-Erofe'ev model
P_i	partial pressure of species i (bar)
$P_{O_2,eq}$	equilibrium partial pressure of O_2 (bar)
T	temperature (K)
T_w	temperature at the wall (K)
U	overall heat transfer coefficient (J/m^2 K s)
X_1	conversion of CuO
X_2	conversion of Cu_2O

Greek letters

ΔH_j	heat of reaction j (J/mol)
ε_b	porosity of the bed
λ_{ax}	axial heat dispersion coefficient (W/m K)
ρ_b	bulk density of the fixed-bed (kg/m^3)

Since Cu-based OCs can be used as a CLC and CLOU material, the challenge lies in determining the regime, in which the heterogeneous reduction or the oxygen uncoupling reactions dominate. Table 1 presents all the potential reactions that may occur in a CH_4–CuO system, including reactions catalyzed by Cu, the heterogeneous reactions with Cu oxides and the oxygen uncoupling reactions of CuO. Although CLOU is predominantly considered for solid fuels processes, the existence of gaseous intermediate products, such as CH_4, H_2 and CO from gasification and pyrolysis reactions, should be accounted for. Also, it has been shown that temperature has a significant effect on the CLC/CLOU performance [10,16]. Therefore, the reaction rates of CLC and CLOU with gaseous fuels need to be examined at a wide temperature range for reactor design purposes. To the best of our knowledge, no systematic studies focusing on this type of analysis have been reported. Moreover, there exists only limited work aimed at investigating the kinetics of reactions with supported CuO/Cu_2O/Cu. The 2-D shrinking core model (SC2) was used by Abad et al. [5,8] and Moghtaderi and Song [24] to describe the kinetics of CuO/Al_2O_3 with CH_4, H_2 and CO (R1′, R5′ and R7′) at 800 °C. Chuang et al. [25–27] and Goldstein and Mitchell [28] proposed a sequential reaction scheme with Cu_2O as the intermediate for the reduction of CuO by H_2/CO (R5–R8), using a 3-D shrinking core model (SC3), as supported by optical microscope images. The SC3 model was also used by Son et al. [29] for predicting the reduction reactivity of CuO by syngas in the temperature range of 350–850 °C. Monazam et al. [30] applied the Avrami-Erofe'ev (AE) model on the kinetics of reaction R5′ (Table 1) at 800–900 °C. Overall, unlike Ni [31–34], most of the aforementioned kinetic studies contain incomplete reaction schemes. A kinetic study examining all the possible reactions involved in the CuO-based CLC process and their kinetic parameters is missing. Moreover, the aforementioned studies only dealt with CLC related reactions, and the kinetics of CuO oxygen uncoupling reaction was not considered.

The kinetics of CuO oxygen uncoupling has been studied independently of other chemical-looping-relevant reactions in the literature. Song et al. [9] investigated the kinetics of CuO/SiO_2 oxygen uncoupling at 800–975 °C and observed that the Avrami-Erofe'ev is the best suited model for the solid-state phenomena occurring. Similarly, Arjmand et al. [15] used the Avrami-Erofe'ev model to match the experimental data of oxygen uncoupling of CuO/$MgAl_2O_4$ at 800–900 °C. Clayton et al. [10,11] integrated thermodynamic and kinetic limitations and the CuO oxygen uncoupling rate was found to be independent of CuO concentration in the temperature range of 800–950 °C. The effect of O_2 partial pressure was also investigated by Adánez-Rubio et al. [35] to describe experimental data at 875–1000 °C. The focus of these studies was mainly on the CuO oxygen uncoupling reaction (R9); while the CLC reactions were not considered. Again, a distinction of the dominance between CLC and CLOU is missing.

In this work, the reactivity of CuO/SiO_2 oxygen carriers was investigated in a fixed-bed reactor. Reactions catalyzed by Cu, the heterogeneous reactions with Cu oxides and the oxygen uncoupling reactions of CuO were studied for a relatively wide range of temperatures (750–980 °C). The sequential reaction scheme of CuO reduction *via* the intermediate Cu_2O was validated by *in situ* X-ray diffraction (XRD). On the basis of fixed-bed and TGA experiments and supplementary characterization techniques, a detailed kinetic network was developed for the reduction step of CuO-based, CH_4-fed CLC or CLOU processes. Validation of the proposed kinetic scheme against experimental data (in fixed-bed and fluidized bed reactors) from the literature and the in-house fixed-bed reactor at a wide range of temperatures was performed. Eventually, a comparison between the rates of all the relevant reactions involved at various temperatures is shown, along with a continuous regime, where the dominant CuO reduction reactions at lower temperatures are replaced by CuO oxygen uncoupling reactions as temperature increases.

2. Experimental

2.1. Oxygen carrier

CuO/SiO_2 OCs were prepared *via* incipient wetness impregnation. Aqueous $Cu(NO_3)_2$ was added to a SiO_2 gel support (Sigma–Aldrich) with an average particle size of 100 μm and BET surface area of 750 m^2/g. The silica gel was pre-dried overnight at 110 °C to remove moisture. The mixture was then stirred at room

Table 1
$CuO–CH_4$ chemical-looping combustion and chemical-looping with oxygen uncoupling reaction schemes.

OC reduction reactions	$CH_4 + 6CuO \rightarrow 3Cu_2O + CO + 2H_2O$	$\Delta H_1 = -8.82E+04$	(R1)
	$CH_4 + 4CuO \rightarrow 2Cu_2O + 2H_2 + CO_2$	$\Delta H_2 = -3.13E+04$	(R2)
	$CH_4 + 2CuO \rightarrow Cu_2O + 2H_2 + CO$	$\Delta H_3 = 1.08E+05$	(R3)
	$CH_4 + 4Cu_2O \rightarrow 8Cu + 2H_2O + CO_2$	$\Delta H_4 = -1.36E+05$	(R4)
	$2CuO + H_2 \rightarrow Cu_2O + H_2O$	$\Delta H_5 = -9.81E+04$	(R5)
	$Cu_2O + H_2 \rightarrow 2Cu + H_2O$	$\Delta H_6 = -7.51E+04$	(R6)
	$2CuO + CO \rightarrow Cu_2O + CO_2$	$\Delta H_7 = -1.39E+05$	(R7)
	$Cu_2O + CO \rightarrow 2Cu + CO_2$	$\Delta H_8 = -1.16E+05$	(R8)
	$4CuO + CH_4 \rightarrow CO_2 + 2H_2O + 4Cu$	$\Delta H_{1'} = -1.82E+05$	(R1′)
	$CuO + H_2 \rightarrow Cu + H_2O$	$\Delta H_{5'} = -8.66E+04$	(R5′)
	$CuO + CO \rightarrow Cu + CO_2$	$\Delta H_{7'} = -1.28E+05$	(R7′)
OC oxygen uncoupling reaction	$4CuO \rightarrow 2Cu_2O + O_2$	$\Delta H_9 = 2.87E+05$	(R9)
Reactions catalyzed by Cu	$CO_2 + CH_4 \leftrightarrow 2CO + 2H_2$	$\Delta H_{10} = 2.47E+05$	(R10)
	$CO + H_2O \leftrightarrow CO_2 + H_2$	$\Delta H_{11} = -4.12E+04$	(R11)
	$CH_4 + 2O_2 \rightarrow CO_2 + 2H_2O$	$\Delta H_{12} = -8.02E+05$	(R12)
	$2H_2 + O_2 \rightarrow 2H_2O$	$\Delta H_{13} = -4.84E+05$	(R13)
	$2CO + O_2 \rightarrow 2CO_2$	$\Delta H_{14} = -5.66E+05$	(R14)
	$CH_4 \rightarrow C + H_2$	$\Delta H_{15} = 7.48E+04$	(R15)
	$CO_2 + C \rightarrow 2CO$	$\Delta H_{16} = 1.73E+05$	(R16)
	$CH_4 + H_2O \rightarrow 3H_2 + CO$	$\Delta H_{17} = 2.06E+05$	(R17)

temperature followed by drying at 120 °C for 12 h and calcination in air at 600 °C for 3 h. In order to increase the total CuO loading, two impregnation steps were performed. The sample obtained after the two impregnation steps was sintered at 950 °C for 6 h to enhance its mechanical strength. The resulting OC was then sieved to particle sizes of 50–150 μm. The stability of the OC was tested in a fixed-bed reactor and TGA for 30 redox cycles, showing good stability and reactivity. The physical properties of the fresh and used oxygen carriers are shown in Table 2.

2.2. Characterization techniques

The active CuO loading in the OC was measured by complete oxygen uncoupling in N_2 in a TGA (NETZSCH STA 449 F3 Jupiter) and in a fixed-bed reactor at 950 °C. Identification of crystallite chemical species and crystallite size change was performed with *in situ* hot-stage X-ray diffraction measurements, in a Bruker D8 Advance power XRD, equipped with a LynxEye-super speed detector. Moreover, measurements in a VG Scientific X-ray Photoelectron Spectroscopy (XPS) were carried out to examine surface properties of fresh and used materials. The pore properties and specific surface area of the oxygen carriers were determined in a Micrometitics ASAP 2020 Accelerated Surface Area and Porosimetry System. The pore size distribution was determined from adsorption/desorption of N_2 at 77 K with the Brunauer–Emmett–Teller (BET) method. All the samples were degassed at 250 °C for 12 h before analysis.

Table 2
Main properties of the fresh and used CuO-based oxygen carriers prepared in this work.

Properties	Unit	Fresh CuO/SiO_2	Used CuO/SiO_2[e]
Active CuO content (TGA)[a]	wt%	36.2	35.9
Active CuO content (fixed-bed)[b]	wt%	37.0	37.2
CuO content on the surface (XPS)[c]	wt%	31.3	28.6
XRD phases	–	CuO, SiO_2	CuO, SiO_2
CuO Crystallite size (XRD)[d]	Å	537.6	548.3
Particle size	μm	50–150	50–150
Pore size[f]	Å	219.5	235.2
Surface area[f]	m^2/g	6.493	5.974

[a] Determined by TGA.
[b] Determined by completely decomposing CuO in fixed bed reactor at 950 °C.
[c] Determined by XPS.
[d] Determined by XRD, from the Scherrer equation.
[e] after 30 redox cycles (10 h) in a fixed-bed reactor.
[f] Determined by BET.

2.3. Experimental apparatus

The fixed-bed experimental setup used in this study is shown in Fig. 1. When operating in CLC conditions, fuel (CH_4) and O_2/Ar are periodically fed to the reactor to simulate chemical-looping reduction and oxidation cycles, with inert gas (Ar) used for purging between cycles. In oxygen uncoupling (OU) mode, pure Ar is fed at high temperatures to prompt the CuO oxygen uncoupling. The sequential gas flow switch (CH_4/Ar → Ar → O_2/Ar → Ar) for CLC and (Ar → O_2/Ar → Ar) for OU, are controlled automatically by mass flow controllers and the total gas flow rate is kept constant for all the cycles. The gas product passes through a condenser to eliminate H_2O and is measured downstream by an on-line mass spectrometer. The reactor pressure is regulated by a back pressure regulator and was kept at 1 atm for all the experiments. The bed temperature is controlled by a tubular furnace and is measured and recorded by a thermocouple placed inside the oxygen carrier bed. The reactivity tests were carried out in the temperature range of 750–980 °C. The temperatures reported in the remaining of this paper refer to the average temperature over the duration of each experiment, for which the maximum fluctuation recorded was 15 °C. Each of the experiments was repeated three times and a good repeatability of the experiments was observed. Additionally, each chemical-looping experiment was performed for up to 30 consecutive redox cycles and reached complete stability after cycle 10. In this study, the experiments of cycle 15 are presented, with error bars for the standard error of the experiments. Table 3 summarizes the experimental conditions used in this study.

3. Analysis of the $CuO–CH_4$ reaction system

The objective of this section is to experimentally explore all the potential reactions that occur in the $CuO–CH_4$ system in the

Table 3
Summary of experimental conditions studied in this work.

Variables	
Reactor I.D.	9.9 mm
OC load	2 g
Total flow rate	100 sccm
Temperature	750–980 °C
Exit reactor pressure	1 atm
Oxidation feed	10%, 20% O_2 in Ar
Reduction feed	10% CH_4 in Ar, 10% H_2 in Ar, 5% CO in Ar
Inert purge	Ar

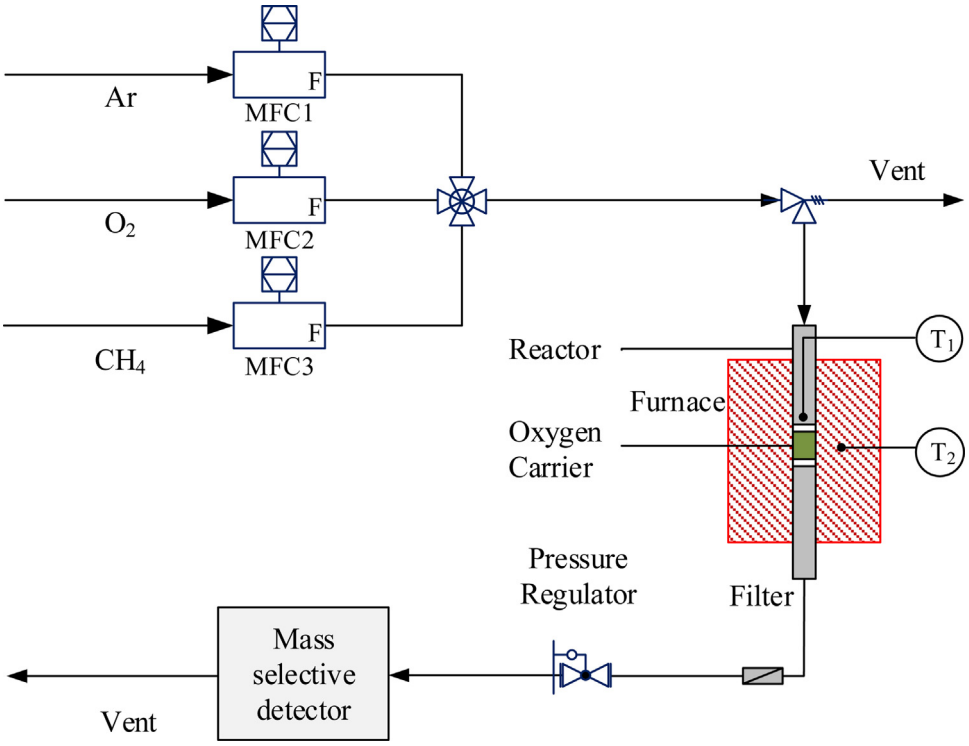

Fig. 1. Fixed-bed chemical-looping reactor setup used in this work.

temperature range of 750–980 °C, supported by other complementary techniques, such as *in situ* XRD, TPR and scanning electron microscopy (SEM). Reactions R1–R14 (Table 1) are considered in this study and are further discussed in this section. The experimental data are analyzed using a 1-D homogeneous model of the corresponding mass and energy balances with axial dispersion, neglecting intra- and inter-particle mass transfer effects [36]. The detailed model equations can be found in the Supporting Information and in previous work [36–38]. The physical properties of the gaseous species can be found in Han et al. [36]. In an effort to minimize the number of kinetic parameters to be estimated, only the kinetic driving force and the Avrami-Erofe'ev exponent *n* were used to fit the model to the experimental data. Dynamic parameter estimation was performed in Matlab™ [39] using nonlinear least-squares with the trust-region-reflective optimization algorithm. Parameter estimation for the kinetic constants for each individual reaction was carried out hierarchically in this study. Firstly, we started with fitting the simpler reactions, for instance, the CuO oxygen uncoupling reaction (R9), and then the catalytic reactions (water gas shift and dry reforming, R10 and R11). Moving forward, the estimation of the kinetics of the reactions between Cu_2O/CuO and H_2/CO (R5–R8) was performed individually. Eventually, the kinetic parameters for the reactions between Cu_2O/CuO and CH_4 (R1–R4) were estimated. For every subsequent reaction scheme the kinetic parameters of all the previously analyzed reactions were kept constant, at the values estimated from their respective analyses.

3.1. Oxygen carrier properties

The properties of the CuO/SiO_2 oxygen carrier, fresh and used, are given in Table 2. Consistent active CuO content was measured in thermogravimetric analysis and fixed-bed reactor testing, with negligible differences between the fresh and used OCs. XRD analysis showed the presence of only SiO_2 and CuO in the samples. The XRD spectra of the fresh OC and the OC after 30 redox cycles in the fixed-bed reactor are quite similar, indicating the absence of spinel formation, during material preparation (high temperature calcination) or reactivity tests in the harsh chemical-looping environment. The CuO crystallite size was also estimated by means of XRD, showing no significant change between the fresh and the used sample (Table 2). Fig. 2 depicts the high resolution Cu2p level XP spectra for the fresh and used CuO/SiO_2 OC. The Cu $2p_{3/2}$ and Cu $2p_{1/2}$ major peaks are in the binding energy range of 934–934.3 and 954–954.2 eV, respectively, identifying that CuO is the only Cu-containing phase and confirming the absence of CuO·SiO_2 spinels. The shaken-up satellites observed at about 9 eV on the high binding energy side of the Cu2p level XP spectra are typical of Cu^{2+} species. The XP spectra of the used sample is observed to shift to higher binding energy by ~0.3 eV (Cu$2p_{3/2}$), which is possibly caused by the interference of the SiO_2 [40]. The XPS-measured CuO content on the surface was 31.3 and 28.6 wt.% for the fresh and used samples, respectively. The obtained pore size and surface area measured by BET for the fresh and used OC are also in a good agreement.

3.2. CuO oxygen uncoupling reaction (R9)

In situ XRD analysis was carried out to investigate the phase transformation during the CuO oxygen uncoupling reaction, as shown in Fig. 3. The XRD patterns were recorded when purging CuO/SiO_2 with pure Ar at 950 °C. The experiments were carried out with a constant flow of 50 sccm of air. Upon reaching 950 °C, the feed gas was switched from air to Ar and recording of the X-ray patterns was initiated. The detection angle, 2θ, was set to the range of 34–45°, as this is where the major Cu, CuO and Cu_2O patterns are located. In the first 6 min, no Cu_2O pattern was detected, indicating the presence of an induction period. This activation period in part justifies the Avrami-Erofe'ev model, as site activation is the initial step of this model [41]. The Cu_2O phase began to show up after 6 min of Ar purging. Cu_2O accumulated coupled with a parallel CuO peak decrease as the Ar purging progressed. The CuO patterns practically disappeared after 12 min of purging, while no Cu was

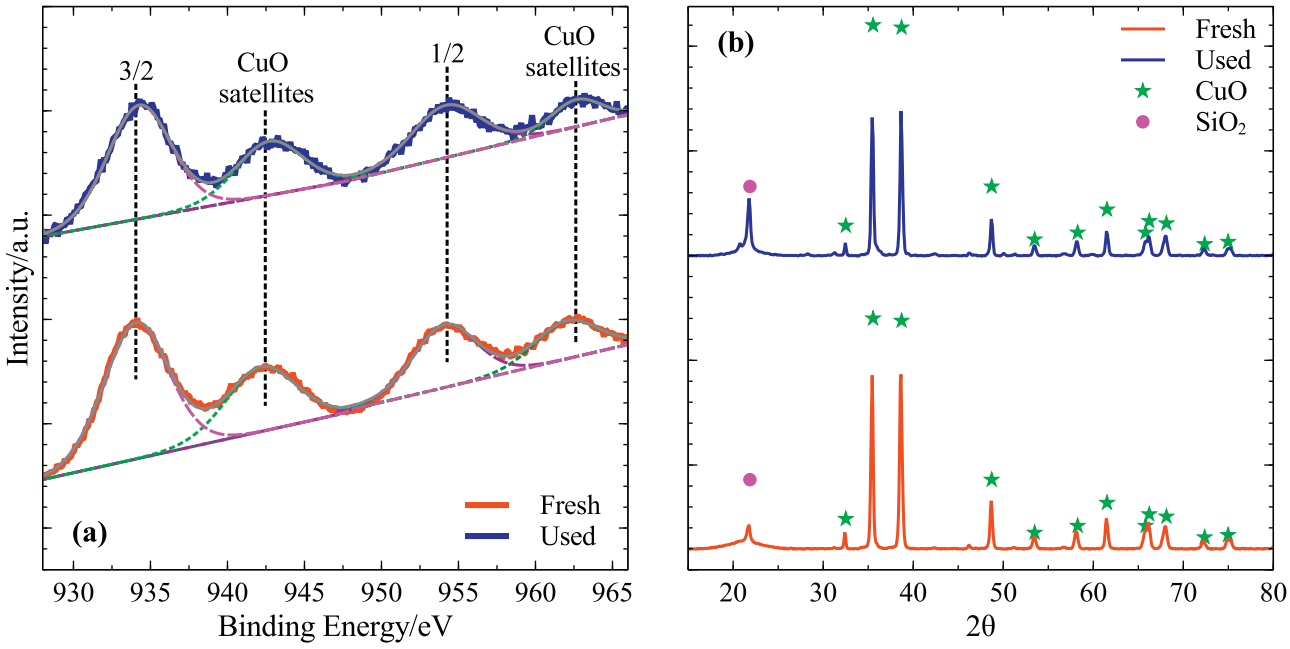

Fig. 2. (a) High-resolution XPS spectrum for the Cu2p region and (b) XRD patterns of the fresh and used CuO/SiO_2 oxygen carrier.

identified in the final sample (Fig. 3). Determination of the kinetics of the oxygen uncoupling of CuO reaction (R9) poses some additional challenges compared to the kinetics of regular CuO reduction, as the rates of R9 are influenced by a combined effect from the activation energy, as well as the oxygen partial pressure driving force. In previous studies [9,15], the Avrami-Erofe'ev model was found to best describe the solid-state kinetics, which is consistent with the XRD observations of Fig. 3. Additionally, the effect of the kinetic rate and the equilibrium partial pressure of oxygen have been analyzed in the literature [10,35]. In this study, the Avrami-Erofe'ev model with dependence on the partial pressure of O_2 was used, as shown in Table 4. This kinetic model was implemented in the 1D dynamic PFR model previously described [32,36] and the pre-exponential factor, $k_{j,0}$, and activation energy, Ea_j, were fitted to fixed-bed experimental data.

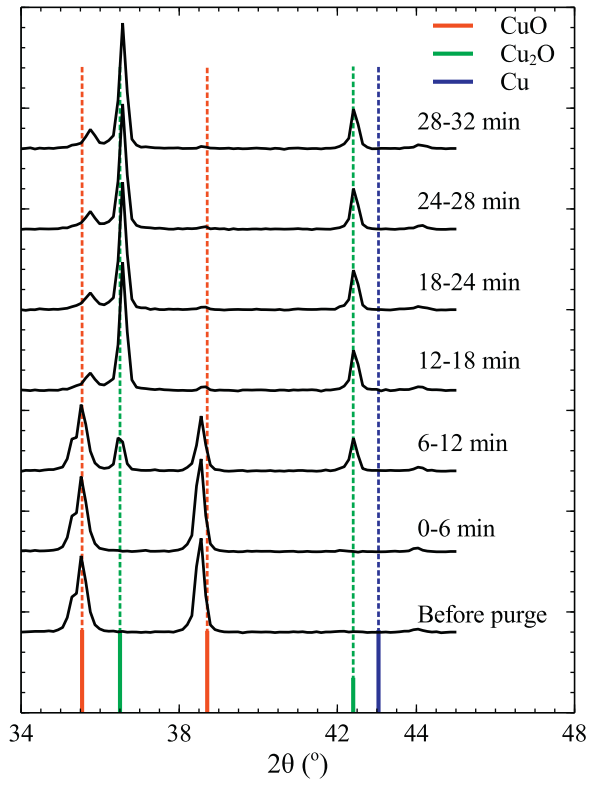

Fig. 3. XRD patterns recorded during the *in situ* isothermal reduction of CuO/SiO_2 under 50 sccm of pure Ar at 950 °C.

Fig. 4(a) shows the comparison between the experimental and modeled O_2 concentrations released from the 2 g sample during an inert gas purge at 4 temperatures (850–975 °C). During this period, CuO spontaneously uncoupled into Cu_2O in the Ar environment, resulting in the release of O_2. Fig. 4(b) presents the O_2 concentration produced from the CuO oxygen uncoupling reaction for extended time, in order to test the capability of the kinetic model to predict the transient behavior until complete OC depletion. As shown in Fig. 4(b), the released O_2 concentration decreased as the availability of CuO dropped and the CuO was almost completely consumed after 20 min of purging with Ar. Fig. 4(c) presents the comparison of the experimental and theoretical equilibrium partial pressure of oxygen. The experimental data correspond to the O_2 concentration in the initial period of CuO uncoupling where the released O_2 concentration is relatively stable (Fig. 4(a)). The measured O_2 is slightly lower than the theoretical value across all four temperatures, indicating that oxygen uncoupling is both thermodynamically and kinetically controlled. The kinetic parameter estimation using the data at 4 temperatures gave the kinetic parameters, shown in Table 4. The Avrami exponent n was estimated at 1.1 and the estimated activation energy was found to be ~140 kJ/mol, which is consistent with the activation energy proposed in the literature [15,42].

3.3. Reactions catalyzed by Cu (R10 and R11)

Cu is recognized as a good catalyst for the water–gas-shift reaction [43,44], however, from the thermodynamic perspective, Jones et al. [45] indicated that noble metals, including, Au, Ag and Cu, are unsuitable for steam reforming of CH_4 (though a good catalyst for steam reforming of methanol [46]). Therefore, the CH_4 steam reforming reaction is neglected in this study. Limited studies with inconclusive findings have been made in terms of the Cu

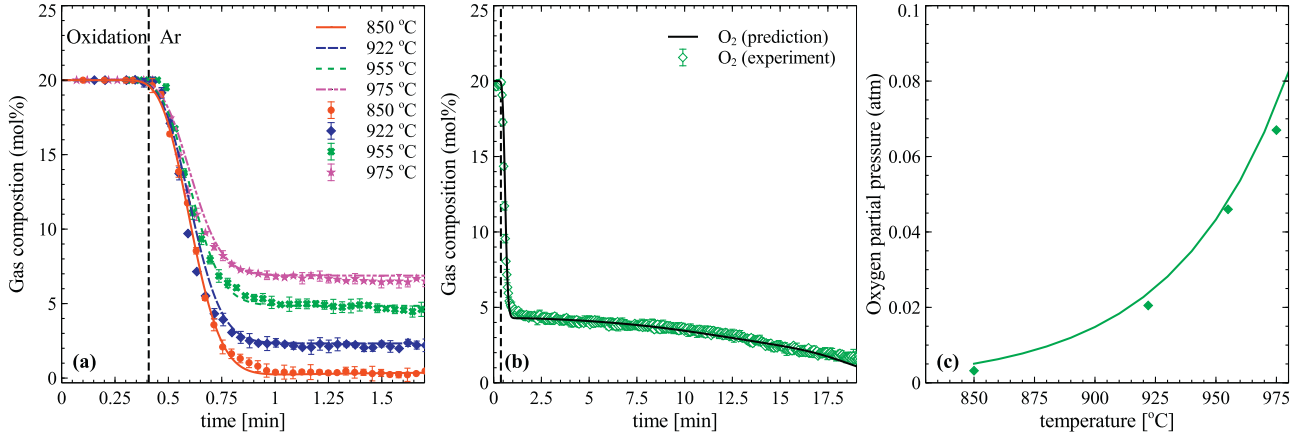

Fig. 4. Experimental and predicted gas profiles of the CuO oxygen uncoupling reaction in the fixed-bed reactor at (a) 850, 922, 955 and 975 °C for 2 min, (b) 955 for 20 min and (c) comparison of the experimental and theoretical equilibrium partial pressure of oxygen.

catalytic activity of the reforming and carbon formation reactions. For instance, some activity of Cu/SiO_2 for the dry reforming reaction was reported by Lewis et al. [47], whereas Fischer and Tropsch [48] detected no activity. In order to clarify this controversy, it is necessary to experimentally test the catalytic reactivity of the Cu/SiO_2 used in this study. For this purpose, experiments were performed with metallic Cu/SiO_2, prepared by completely reducing the CuO/SiO_2 in an atmosphere of H_2. Experiments were performed with this Cu/SiO_2 catalyst in a fixed bed fed with CH_4, CO_2 and H_2.

In separate experiments, 10% CH_4/Ar, 10% CH_4 + 10% CO_2/Ar and 10% CO_2 + 10% H_2/Ar were fed to the system to initiate CH_4 decomposition (R15), dry reforming (R10) and reverse water–gas-shift reactions (R11), respectively. Experiments at 800, 850 and 900 °C were performed to obtain a reliable estimation of the Arrhenius parameters with minimal deviation. The activity of the Cu/SiO_2 material for the CH_4 decomposition reaction was examined first. 10% CH_4 was fed through an empty, clean reactor and through a reactor packed with 2 g Cu/SiO_2 at temperatures up to 900 °C, respectively. Only minor amounts of H_2 were measured in both cases. Therefore, Cu/SiO_2 is not an active catalyst for the CH_4 decomposition reaction, which was neglected in this study. This conclusion is consistent with other literature findings [12,26,49], where no H_2 signal variation along the thermal scan (up to 900 °C) was detected in TPR studies [12,49]. It should be noted, however, that this catalyst was observed to be somewhat active in terms of decomposing CH_4 at higher pressures [50]. Moreover, reduced CuO with other supports, such as Al_2O_3, has shown CH_4 decomposition activity when OC conversions were higher than 75% [51,52]. Catalytic properties, support and experimental particularities are the likely reasons for these discrepancies.

In order to analyze the water–gas-shift reaction (R11) catalyzed by Cu/SiO_2, a gas mixture of 10% CO_2 + 10% H_2/80% Ar was fed to the reactor. Fig. 5 presents the comparison of the experimental and predicted gas profiles at three different temperatures (800, 850 and 900 °C). CO concentrations of about 2.5, 3.5 and 5% were generated at 800, 850 and 900 °C, respectively. Choi and Stenger [53] compared the possible rate expressions for the water–gas-shift reaction and found that the first order reversible rate expression was sufficient to fit the experimental data with high accuracy. Therefore, the first order reversible rate expression is used in this study, shown in Table 4. Parameter estimation was carried out to fit the experimental data across the three temperatures. The activation energy and pre-exponential factor were estimated and found to consistently describe temperature effects, shown in Table 4. The parity diagram of the Arrhenius law [54] for all the reactions considered in this study is shown in the Supporting Information.

A gas mixture of 10% CO_2/10% CH_4/80% Ar was used to study dry reforming (R9) in the fixed-bed reactor (Fig. 6). As H_2 is one of the products from the dry reforming reaction, the water–gas-shift reaction must also be considered in this system. El Solh et al. [55] indicated that the adsorption of CH_4 and the adsorption of CO_2 contribute significantly to the dry reforming kinetics for the Ni catalyzed system. However, most of the kinetic studies of the dry reforming reaction are based on Ni, Ru, Rh and Pd catalysts [56–58]. Therefore, due to a lack of relevant adsorption parameters, the first order reversible rate expression was used in this study. With the estimated water gas shift kinetic variables (shown in Table 4), the kinetic parameters of the dry reforming reaction were estimated for the experimental data carried out at three temperatures and is shown in Table 4.

3.4. Reactions of H_2, CO and CH_4 with Cu_2O (R6, R8 and R4)

In terms of gas–solid reactions, unlike NiO [32,41], CuO reactions are more complicated due to the multiple oxidation states

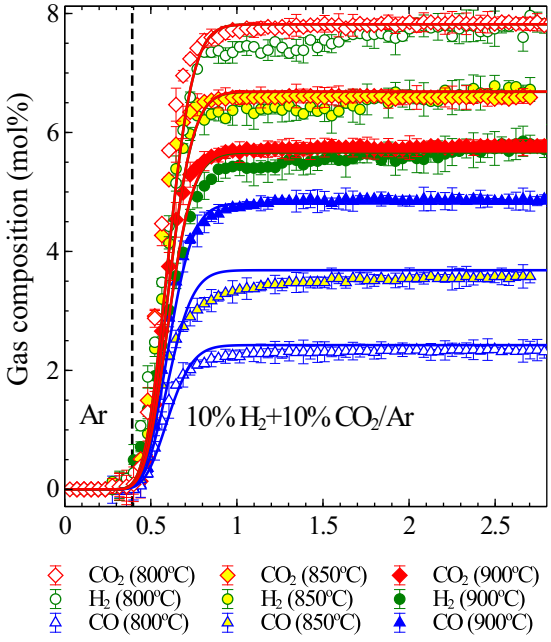

Fig. 5. Experimental and predicted gas profiles of the water–gas-shift reaction catalyzed by Cu/SiO_2 in the fixed-bed reactor at 800, 850 and 900 °C.

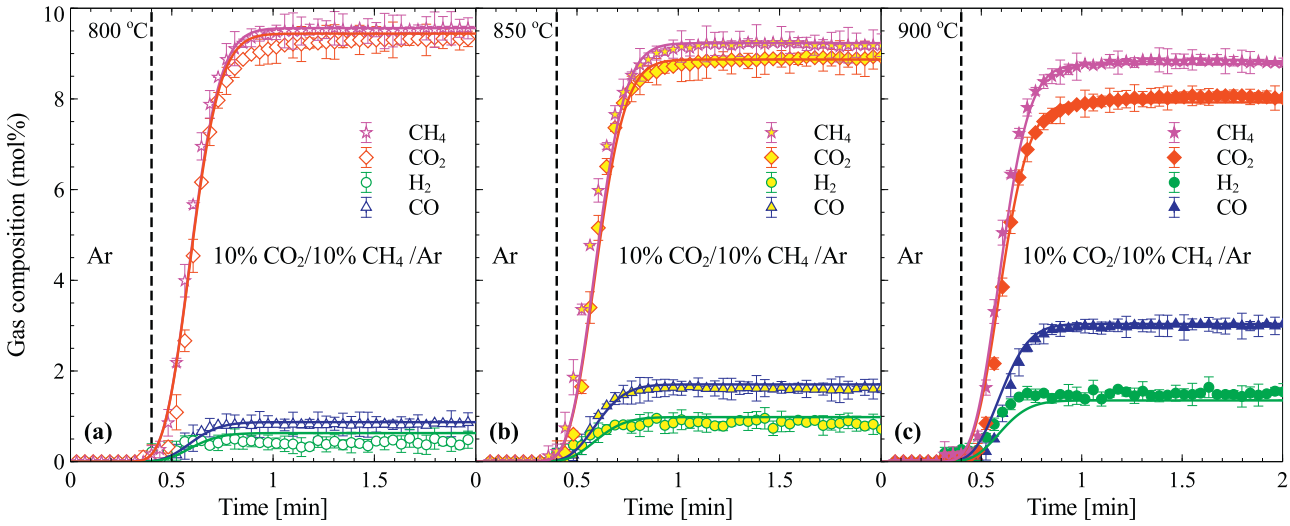

Fig. 6. Experimental and predicted gas profiles of the dry reforming reaction catalyzed by Cu/SiO_2 in the fixed-bed reactor at (a) 800, (b) 850 and (c) 900 °C.

of Cu. There exist sequential reaction schemes for CuO reduction with CO and H_2, involving Cu_2O as the intermediate [25,26,28] or a direct one-step reaction scheme [5]. Goldstein and Mitchell [28] and Chuang et al. [25,26] proposed cascading sequential steps for the reduction of CuO by H_2 and CO at high temperatures, however the reduction reaction of supported CuO with CH_4 is unclear. Therefore, an *in situ* XRD approach was used in order to examine the actual reaction steps and the intermediate Cu oxide phases involved. Fig. 7 presents the XRD patterns recorded during the *in situ* reduction of CuO/SiO_2 with 50 ml/min, 4% CH_4/Ar and 4% H_2/Ar mixtures at 800 °C. Similar to the CuO oxygen uncoupling reaction, during the first 8 min, no major changes were seen. Again, there is clearly an induction period for the reduction of CuO/SiO_2 by H_2 and CH_4, as is commonly observed in the reduction of NiO in previous studies [31,41]. The Avrami-Erofe'ev model appears to be an appropriate model, as it involves a step of activation of sites and formation of nuclei. During the reduction period, which lasted 12–16 min for CH_4/Ar and 8–12 min for H_2/Ar, the presence of CuO lines began to fade, while simultaneously lines for Cu_2O began to be detected. As the reduction proceeds, the newly formed Cu_2O was further reduced to Cu in both cases, as detected in the reduction period from 16 to 32 min. Overall, a multi-step sequential reaction scheme was observed, with Cu_2O as the intermediate phase. Therefore, reactions R5 and R6 are proposed as the reduction reactions of CuO with H_2 and reactions R7 and R8 are the reduction reactions with CO. As shown later, in fixed-bed CH_4–CuO experiments, relatively high CO concentrations were present in the outlet gas together with CO_2 and unreacted CH_4 (Fig. 10), particularly at low

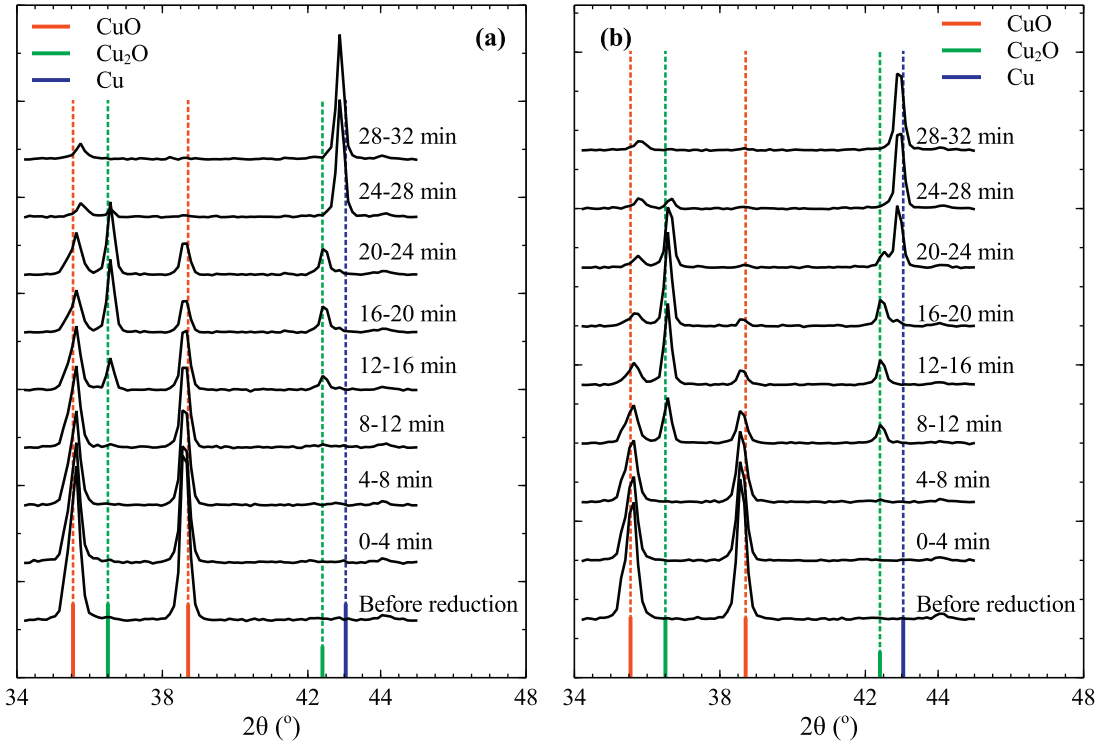

Fig. 7. XRD patterns recorded during the *in situ* isothermal reduction of CuO/SiO_2 under 50 sccm of (a) 4% CH_4/Ar and (b) 4% H_2/Ar mixture at 800 °C.

Table 4
Pre-exponential factors, activation energies, and confidence interval (95%) of the proposed model (units are reported in the Notation).

	Pre-exponential factor ($k_{j,0}$)			Activation energy (Ea_j, kJ/mol)			Activation energy of relevant studies (Ea_j, kJ/mol)	Kinetic expression
	Estimate	LL	UL	Estimate	LL	UL		
R1	7.58E−02	6.30E−02	8.86E−02	9.43E+01	8.42E+01	1.04E+02	–	$r_1 = a_0 k_1 n(1-X_1)(-\ln(1-X_1))^{1-1/n} C'_{CH_4} C'_{CuO}$
R2	2.42E+06	2.25E+06	2.59E+06	2.17E+02	2.06E+02	2.27E+02	–	$r_2 = a_0 k_2 n(1-X_1)(-\ln(1-X_1))^{1-1/n} C'_{CH_4} C'_{CuO}$
R3	7.76E+03	7.25E+03	8.27E+03	1.68E+02	1.51E+02	1.85E+02	–	$r_3 = a_0 k_3 n(1-X_1)(-\ln(1-X_1))^{1-1/n} C'_{CH_4} C'_{CuO}$
R4	5.26E+03	5.02E+03	5.49E+03	1.73E+02	1.62E+02	1.84E+02	–	$r_4 = a_0 k_4 n X_1(1-X_2)(-\ln(1-X_2))^{1-1/n} C'_{CH_4} C'_{CuO}$
R5	1.50E+02	1.18E+02	1.82E+02	6.51E+01	5.25E+01	7.77E+01	43–73 [25]	$r_5 = a_0 k_5 n(1-X_1)(-\ln(1-X_1))^{1-1/n} C'_{H_2} C'_{CuO}$
R6	4.96E+01	3.54E+01	6.38E+01	6.98E+01	5.52E+01	8.44E+01	34–54 [25]	$r_6 = a_0 k_6 n X_1(1-X_2)(-\ln(1-X_2))^{1-1/n} C'_{H_2} C'_{CuO}$
R7	6.62E+01	2.21E+01	1.10E+02	1.01E+02	9.52E+01	1.07E+02	>80 [26]	$r_7 = a_0 k_7 n(1-X_1)(-\ln(1-X_1))^{1-1/n} C'_{CO} C'_{CuO}$
R8	1.16E+03	5.42E+02	1.78E+03	1.27E+02	1.17E+02	1.37E+02	44–128 [26]	$r_8 = a_0 k_8 n X_1(1-X_2)(-\ln(1-X_2))^{1-1/n} C'_{CO} C'_{CuO}$
R9	8.81E+04	7.76E+04	9.86E+04	1.41E+02	1.24E+02	1.58E+02	62 [10], 139 [15], 315 [9], 176 [9]	$r_9 = a_0 k_9 n(1-X_1)(-\ln(1-X_1))^{1-1/n} (P_{O_2,eq} - P_{O_2}) C'_{CuO}$
R10	6.64E+01	6.33E+01	6.95E+01	1.28E+02	1.27E+02	1.29E+02	–	$r_{10} = k_{10} \left(P_{CO}^2 P_{H_2}^2 - \frac{P_{CO_2} P_{CH_4}}{K_{10}} \right) C_{Cu}$
R11	2.35E+01	1.25E+01	3.44E+01	9.85E+01	9.03E+01	1.07E+02	–	$r_{11} = k_{11} \left(P_{CO_2} P_{H_2} - \frac{P_{CO} P_{H_2O}}{K_{11}} \right) C_{Cu}$
R12	2.70E+03			1.25E+02			–	$r_{12} = \frac{k_{12}(600 P_{O_2})^{0.5} P_{CH_4}}{1+(600 P_{O_2})^{0.5} + 500 P_{CO_2} + 950 P_{H_2O}}$
R13	1.91E+00			7.75E+01			–	$r_{13} = \frac{k_{13} K_{H_2}^{0.5} P_{H_2}^{0.5} P_{O_2}^{0.5}}{0.5 K_{13} K_{H_2}^{0.5} P_{H_2}^{0.5} + K_{O_2,13} P_{O_2}^{0.5} (1+K_{H_2}^{0.5} P_{H_2}^{0.5})}$
R14	5.00E−02			5.07E+01			–	$r_{14} = \frac{k_{14} P_{CO}^{0.5} P_{O_2}^{0.5}}{(1+K_{CO} P_{CO} + \sqrt{K_{O_2,14} P_{O_2}})^2}$

UL, upper limit; LL, lower limit of approximate 95% confidence interval. Reactions R12–R14 were not fitted to experimental data; the reported values from the corresponding literature [59–61] were used, as described in Section 3.7.

temperature; thus, a CuO–CH_4 reaction scheme with CO and H_2 as the partial combustion products was used (reactions R1–R4).

For the purpose of obtaining an accurate set of kinetic parameters for the Cu_2O reactions (R4, R6 and R8), the lower oxide, Cu_2O, was prepared by completely uncoupling CuO/SiO_2 in a fixed-bed reactor at 950 °C in an atmosphere of pure Ar for an extended time. When the CuO oxygen uncoupling was complete, the bed was cooled with continuous purge of Ar. 10% H_2/Ar, 5% CO/Ar and 10% CH_4/Ar were then introduced to the Cu_2O/SiO_2 bed at three temperatures (800, 825 and 850 °C), respectively. Parameter estimation was first carried out to estimate the kinetic parameters of the reactions between Cu_2O and H_2, CO or CH_4 (R6, R8 and R4).

Fig. 8 presents the comparison of the predicted and experimental gas profiles from the Cu_2O reduction reaction with H_2, CO and CH_4. It should be noted that accurate calibration and measurement of H_2O in the spectrometer are difficult. Therefore, for the tests with H_2 as the fuel source, the H_2O profile is not measured while the presence of H_2 after achieving complete reduction is the only measured gas profile, as shown in Fig. 8(a). About 10 min reduction was required to completely reduce Cu_2O/SiO_2 by the diluted H_2. As shown in Fig. 8(b), most of the CO was converted to CO_2 with marginal amounts of unreacted CO present. As for the Cu_2O–CH_4 reaction (R4), most of the CH_4 left the reactor unreacted with only small amounts of CO_2 measured (Fig. 8(c)). Considering that the same OC was used at similar operating conditions for the CuO oxygen uncoupling study (Section 3.1), as well as the *in situ* XRD indication of the existence of an activation step, the Avrami-Erofe'ev model with exponent $n = 1.1$ was used for the Cu_2O reductions also. The kinetic expressions and their corresponding kinetic parameters for reactions R4, R6 and R8 are shown in Table 4.

3.5. Reactions of H_2 and CO with CuO (R5 and R7)

After obtaining kinetic parameters for the reactions between Cu_2O and H_2/CO, experiments were performed by flowing 10% H_2/Ar and 5% CO/Ar to the bed of CuO, to investigate the kinetics of reactions between CuO and H_2 or CO (R5 and R7, respectively). Shown in Fig. 9(a), the H_2 breakthrough started at ~17 min of reduction of the CuO/SiO_2. Similar H_2 profiles were measured at the three temperatures (Fig. 9(a)). For the experiment between CuO/SiO_2 and CO, most of the CO was converted to CO_2 (Fig. 9(b)). On the basis of the estimated kinetics of all the relevant reactions (R4, R6 and R8–R11), the estimation of the kinetics of reactions of CuO with H_2 and CO (R5 and R7, respectively) was carried out. The calculated activation energies for R5–R8, shown in Table 4, are in the vicinity of the values reported in the relevant literature, 43–74 kJ/mol [25] (R5), 34–54 kJ/mol [25] (R6), >80 kJ/mol [26] and 20 kJ/mol [28] (R7), 44–128 kJ/mol [26] and 25 kJ/mol [28] (R8).

3.6. Reactions of CH_4 with CuO (R1–R3)

Lastly, a series of experiments between CuO/SiO_2 and diluted CH_4 were carried out at three temperatures (800, 825 and 850 °C) in the fixed-bed reactor, as shown in Fig. 10. A large amount of CH_4 (~30 mol.% of the CH_4 feed) remained unreacted at 800 °C, however, more CH_4 was consumed as the temperature increased. Corbella et al. [12] showed that no chemical reaction occurs at temperatures lower than 750 °C with CuO/SiO_2 as the OC and CH_4 as the fuel, supported by thermal scan TPR analysis, which agrees in part with the experimental results of this work. Again, the Avrami-Erofe'ev model with $n = 1.1$ was used for the reactions between CuO and CH_4 (reactions R1–R3). By employing the estimated kinetics for all the possible reactions (R4–R14), estimation of the kinetic parameters for only R1–R3 was carried out. As shown in Fig. 10, the model is shown to be capable of representing the experimental data quite

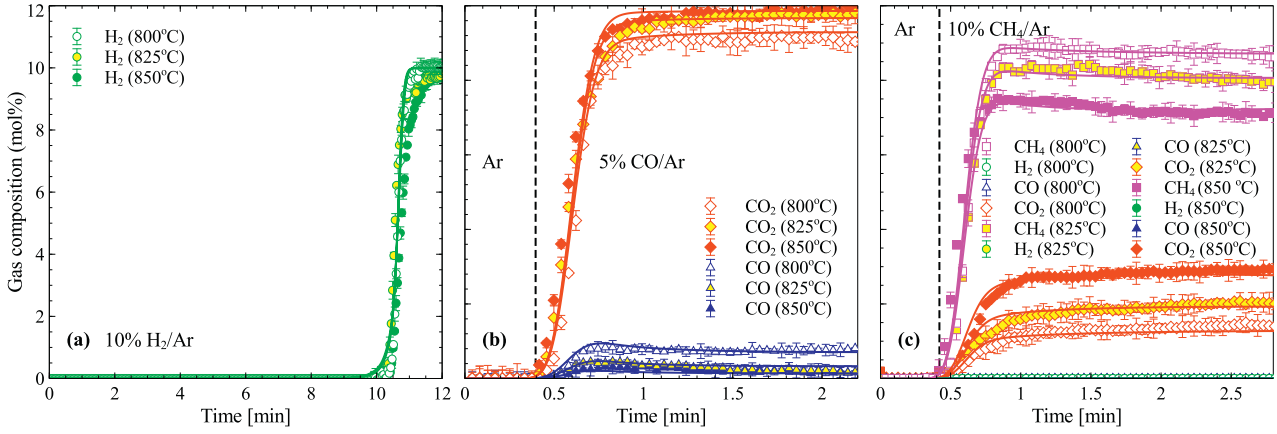

Fig. 8. Experimental and predicted gas profiles using (a) Cu_2O/SiO_2 and 10% H_2/Ar, (b) Cu_2O/SiO_2 and 5% CO/Ar and (c) Cu_2O/SiO_2 and 10% CH_4/Ar in the fixed-bed reactor at 800, 825 and 850 °C.

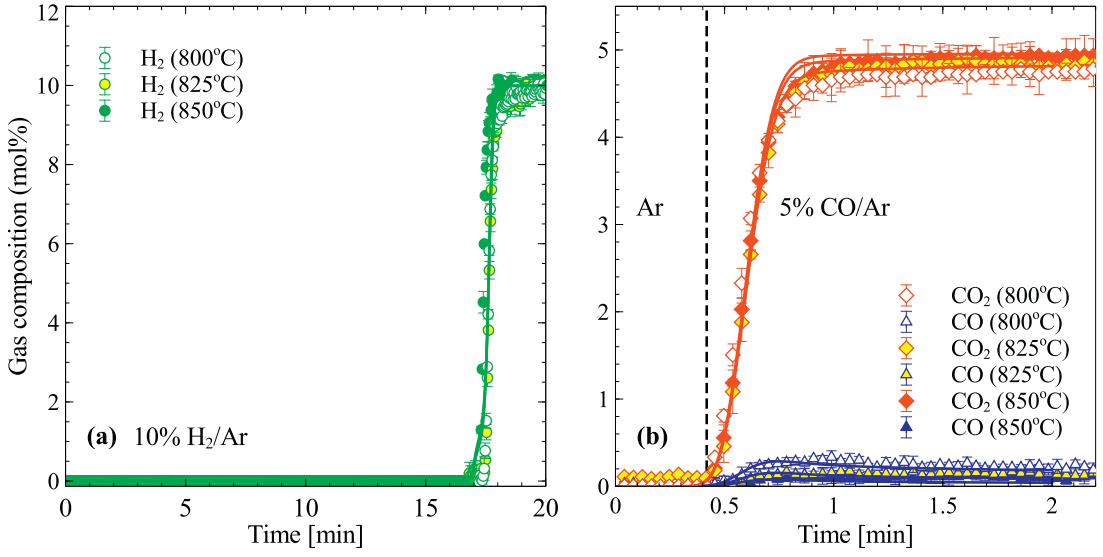

Fig. 9. Experimental and predicted gas profiles using CuO/SiO_2 and (a) 10% H_2/Ar and (b) 5% CO/Ar in the fixed-bed reactor at 800, 825 and 850 °C.

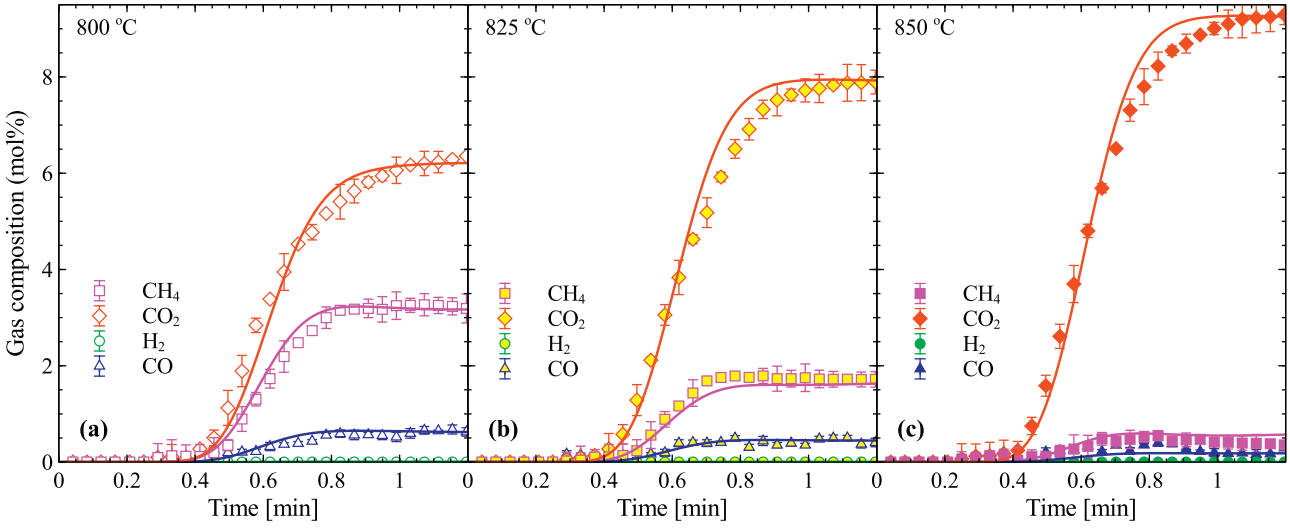

Fig. 10. Experimental and predicted gas profiles of the CLC/CLOU system using CuO/SiO_2 and CH_4 in the fixed-bed reactor at (a) 800, (b) 825 and (c) 850 °C.

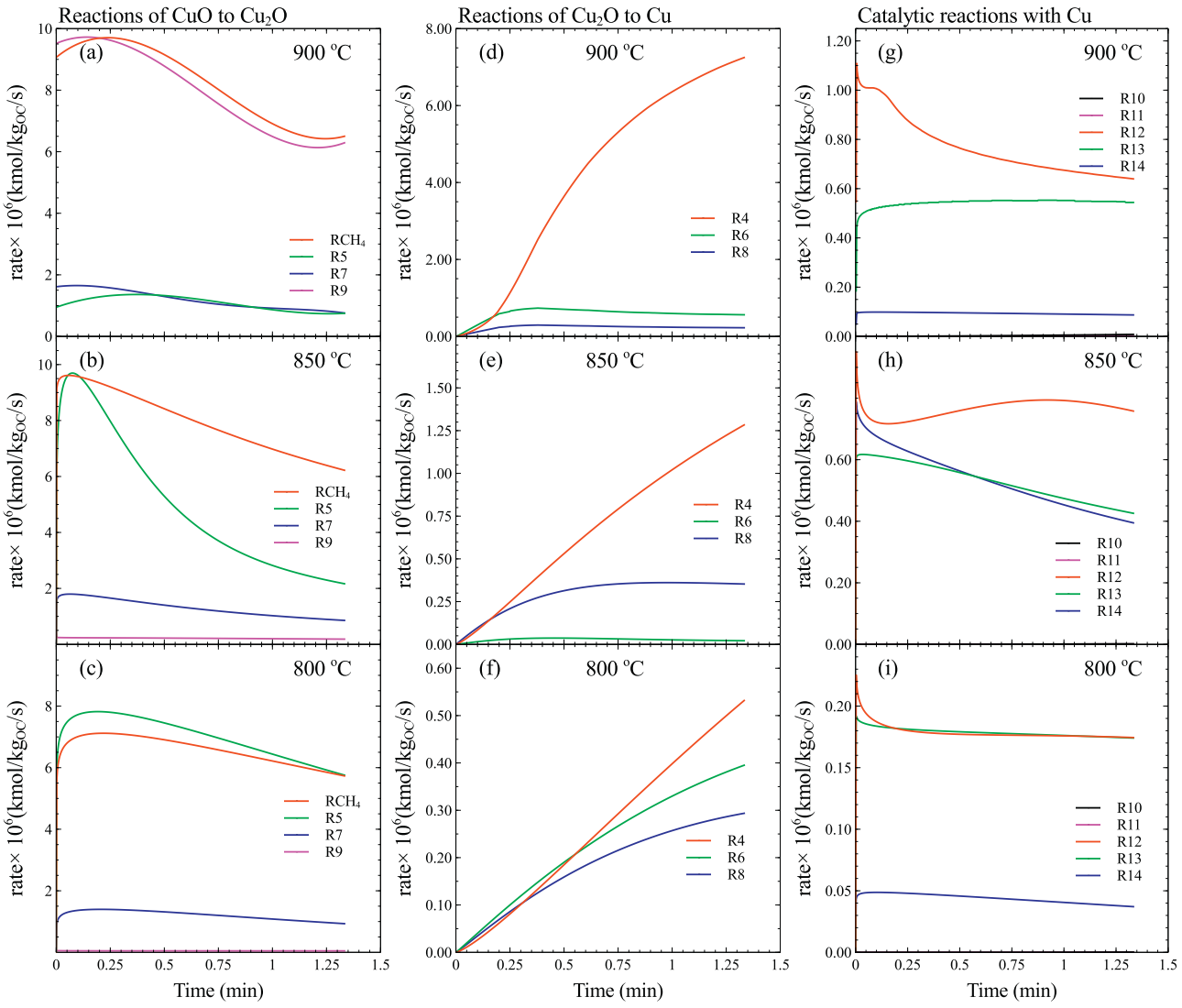

Fig. 11. Average (over reactor volume) reaction rates at 800, 850 and 900 °C. Reactions R1–R14 are as given in Table 1 and the corresponding rate expressions are shown in Table 4.

accurately for the entire range of temperatures studied. The estimated activation energies and pre-exponential factors for reactions R1–R3 are shown in Table 4.

3.7. Summary of reaction scheme and kinetic network

Overall, the complete reaction scheme for CH_4-fed CLC/CLOU with a CuO/SiO_2 oxygen carrier is shown in Table 4. The Avrami-Erofe'ev model with the Avrami exponent n of 1.1 is utilized for all the gas–solid reactions (R1–R8) and the CuO oxygen uncoupling reaction (R9). The first order reversible expression is used for the dry reforming (R10) and water–gas-shift reactions (R11). The kinetic expressions and parameters for the fast gas phase combustion reaction between O_2 and CH_4, O_2 and CO, and O_2 and H_2 were obtained from Veldsink et al. [59], Ayastuy et al. [60] and Avgouropoulos and Ioannides [61], respectively. It should be noted that the gas phase combustion reaction between CH_4 and O_2 can be achieved through partial and/or complete oxidation pathways. However, due to the fast kinetics of the gas phase combustion reactions and the property of CuO to act as a continuous oxygen source, the partial oxidation reaction of CH_4 was not considered in this study. A summary of all the relevant kinetic expressions and their estimated kinetic parameters and fit quality statistics, as well as a comparison with kinetic parameters from relevant studies are shown in Table 4.

Fig. 11 illustrates the significance of each reaction and its dependency on temperature. This is an excerpt of the results generated in this work and presents a comparison of the transient rate profiles of all the reactions at 800, 850 and 900 °C, as estimated for the in-house fixed bed reactor. In Fig. 11, the reactions are categorized as CuO reduction reactions to Cu_2O (R1, R2, R3, R5, R7 and R9 of Table 1), Cu_2O reduction reactions to Cu (R4, R6 and R8) and reactions catalyzed by Cu (R10–R14). The rate of the reactions between CuO and $CH_4/H_2/CO$ remain relatively constant when the bed temperature increases from 800 to 850 °C (Fig. 11(b) and (c)). For the same temperature rise, the CuO oxygen uncoupling reaction rate increases significantly. However, the rates of CuO reduction with CH_4 and H_2 are still significant at 900 °C (Fig. 11(a)), indicating that CLOU cannot be decoupled from CLC. Also, the rates of Cu_2O reduction and catalytic reactions, although smaller cannot be neglected.

4. Further application of the proposed kinetics

In this section, the proposed kinetics is extended to predict the experiments carried out in the fixed-bed reactor at temperatures

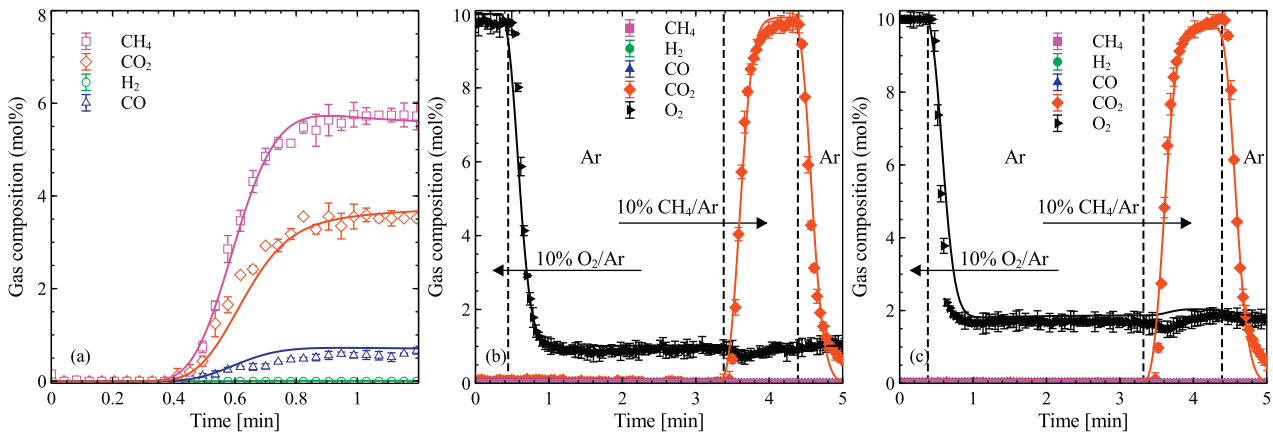

Fig. 12. Experimental and predicted gas profiles of the CLC/CLOU system using CuO/SiO_2 and CH_4/Ar in the fixed-bed reactor at (a) 760 °C, (b) 900 °C and (c) 925 °C.

exceeding 850 °C, where the CuO oxygen uncoupling reaction rate is significant, and at a lower temperature (<800 °C), where the CuO oxygen uncoupling reaction is negligible and CLC reactions are slow. Furthermore, the same kinetic network was used to simulate the experimental data from the literature in fixed-bed and semi-batch fluidized bed reactors, with the intention to analyze the generality and validity of the proposed kinetic network. A three-phase fluidized bed model developed previously was used here [38,62]. It should be noted that the predictions shown in the following do not involve any parameter estimation; instead, they are the pure predictions from the process models of previous studies [36,62] and the kinetic network reported here.

CLC and CLOU experiments were carried out at 760, 900 and 925 °C, shown in Fig. 12. The OC shows slight activity at 760 °C with 60% of CH_4 remaining unreacted and the CO_2 selectivity being lower than 40% (Fig. 12(a)). At high temperatures, however, the CuO oxygen uncoupling reaction became dominant (Fig. 12(b) and (c)). Small amounts of O_2 were generated from the CuO during the inert purge and reduction periods. As shown in Fig. 12(b) and (c), 1.2 mol.% and 1.7 mol.% O_2 were produced in the purge phase at 900 and 925 °C, respectively, and were very accurately predicted by the model. All of the CH_4 was consumed through the reaction with CuO and with the released O_2 and, thus, there was no CH_4 detected during the reduction phase. Consumption of the gaseous O_2 shifted the equilibrium of the CuO oxygen uncoupling reaction to the right, thus no significant variation of O_2 was observed.

Table 5
Experimental conditions and oxygen carrier (OC) properties of the literature reported CLC/CLOU data studied.

Author	Corbella et al. [12]	Arjmand et al. [16]
Reactor type	Fixed-bed reactor	Fluidized-bed reactor
T (°C)	800	900
P (atm)	~1	~1
CuO/Support	16% CuO/SiO_2	40% CuO/α–Al_2O_3
OC load (g)	20	15
Particle size (μm)	200–400	125–180
Surface area (m^2/g)	38	4.1
I.D. (m)	0.016	0.022
Bed depth (m)	0.06631	0.01644
Reactor height (m)	0.34	0.5
Gas flow rate (m^3/s)	2.1667E−07	7.5E−06
CH_4 composition	100%	100%
Bulk density (kg/m^3)	1500*	2400

* Assumed value.

Moreover, the rise in temperature caused by the exothermic nature of the gas phase combustion reaction between CH_4 and O_2 shifts the thermodynamic equilibria and in turn increases the O_2 concentration; therefore, no significant drop in O_2 concentration was observed.

Further evaluation of the effectiveness and holistic nature of the proposed kinetic network was carried out by applying the model to predict relevant experimental data found in the literature. Table 5 presents a summary of two relevant sets of CLC/CLOU

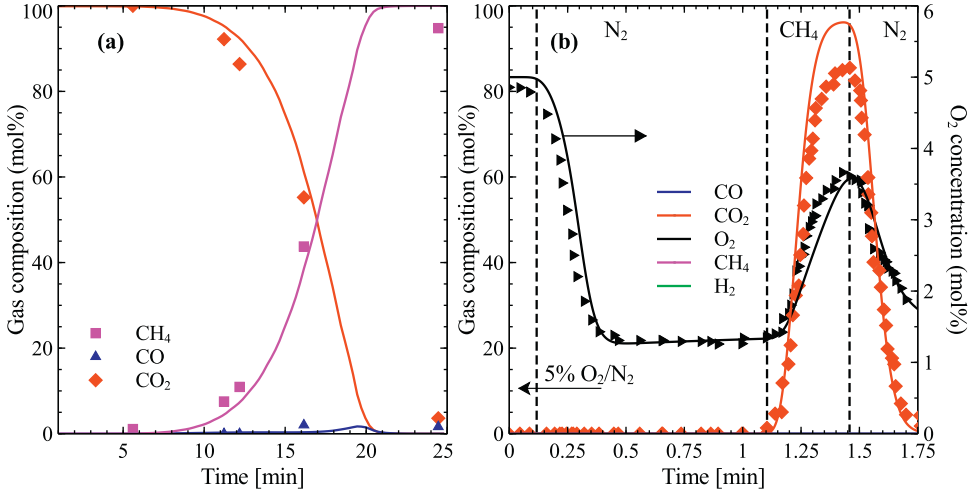

Fig. 13. Experimental and predicted gas profiles of the CLC/CLOU system using (a) CuO/SiO_2 and CH_4 in a fixed-bed reactor at 800 °C and (b) CuO/α-Al_2O_3 and CH_4 in a semi-batch fluidized bed reactor at 900 °C; experimental data from (a) Corbella et al. [12] and (b) Arjmand et al. [16].

experimental data conducted in a fixed-bed reactor and a semi-batch fluidized bed reactor using CH_4 as the fuel and Cu-based OCs. Corbella et al. [12] performed reactivity tests of CuO/SiO_2 OC in a fixed-bed reactor for up to 20 redox cycles. Their experimental data of the 5th cycle were chosen in this study, as there was no significant thermal sintering effect on the gas profile up to this cycle. Fig. 13(a) shows the comparison between experimental data and model predictions at 800 °C. The CO_2 stream is the exclusive product before the CH_4 breakthrough and when the OC conversion is low. As the reactions progress and the CuO to Cu_2O conversion reaches completion, CH_4 breaks through, CO_2 concentration drops rapidly and trace amounts of CO appear. The prediction of the overall trend of this set of data by the model is satisfactory (Fig. 13(a)). Moreover, the predicted conversion of CuO and Cu_2O are both 100% after reduction, which is consistent with the XRD analysis by Corbella et al. [12], who showed that metallic Cu was the only Cu-containing phase at the end of the reduction stage.

The proposed kinetic model was also used to predict the experimental data carried out in the fluidized bed unit designed by Arjmand et al. [16]. The process model from previous work [62] successfully predicted the gas composition carried out in the same unit with $Ni/NiAl_2O_4$ OC [63]. Arjmand et al. [16] performed experiments at 900 °C, where the CuO oxygen uncoupling reaction was significant. Fig. 13(b) presents the comparison of the experimental data of Arjmand et al. [16] and the model predictions. Nearly 1.5 mol.% O_2 was produced during the inert purge. About 3.8 mol.% O_2 concentration was present in the reduction phase caused by the shift of the thermodynamic equilibrium. Complete combustion was achieved and CO_2 was the only carbon-containing species, as accurately predicted by the model. The overall O_2 concentration generated from the purging and reduction periods is also well captured by this model. It should be noted that in Fig. 13, the model results satisfy mass balance, whereas the experimental data do not.

5. Conclusions

A comprehensive kinetic scheme was proposed for the copper oxide-based chemical-looping combustion and chemical-looping with oxygen uncoupling processes, in a relatively wide reaction temperature range (750–980 °C). Analysis of experiments with a CuO/SiO_2 oxygen carrier performed in-house in a fixed-bed reactor and *in situ* XRD isothermal scans, revealed the existence of the following reactions: heterogeneous CuO reduction reactions by $CH_4/CO/H_2$ with Cu_2O as the intermediate, CuO oxygen uncoupling, water–gas-shift, dry reforming and gas phase combustion reactions. The experimentally determined kinetic parameters were shown to be close to the literature reported values. Through a rate comparison of all the reactions involved at 800, 850 and 900 °C, it was revealed that in terms of converting CuO to Cu_2O, all the relevant reactions rates remain relatively constant as the temperature rises. However, the rate of CuO oxygen uncoupling becomes significantly higher when reaction temperature reaches 900 °C, while the increase in the rates of the reactions between CuO and $H_2/CO/CH_4$ is less profound. The kinetic and process models reported here are capable of predicting the continuous CuO CLC/CLOU reactions regime. Thus, they can be used with confidence for process and reactor design studies.

Acknowledgment

This material is based upon work supported by the National Science Foundation under Grant No. 1054718.

Appendix A. Supplementary data

Supplementary data associated with this article can be found, in the online version, at http://dx.doi.org/10.1016/j.apcatb.2014.10.067.

References

[1] T. Mattisson, A. Lyngfelt, H. Leion, Int. J. Greenh. Gas Control. 3 (2009) 11–19.
[2] S. Cheah, K.R. Gaston, Y.O. Parent, M.W. Jarvis, T.B. Vinzant, K.M. Smith, et al., Appl. Catal. B: Environ. 134-135 (2013) 34–45.
[3] T. Mattisson, ISRN Chem. Eng. 2013 (2013) 1–19.
[4] J. Adánez, A. Abad, F. García-Labiano, P. Gayán, L.F. de Diego, Prog. Energ. Combust. 38 (2012) 215–282.
[5] A. Abad, J. Adánez, F. García-Labiano, L.F. de Diego, P. Gayán, J. Celaya, Chem. Eng. Sci. 62 (2007) 533–549.
[6] J. Adánez, L.F. de Diego, F. García-Labiano, P. Gayán, A. Abad, J.M. Palacios, Energy Fuels 18 (2004) 371–377.
[7] L.F. de Diego, F. Garcıá-Labiano, J. Adánez, P. Gayán, A. Abad, B.M. Corbella, et al., Fuel 83 (2004) 1749–1757.
[8] F. García-Labiano, L.F. de Diego, J. Adánez, P. Gayán, Ind. Eng. Chem. Res. 43 (2004) 8168–8177.
[9] H. Song, K. Shah, E. Doroodchi, Energy Fuels 28 (2014) 173–182.
[10] C.K. Clayton, K.J. Whitty, Appl. Energy 116 (2014) 416–423.
[11] C. Clayton, H. Sohn, K. Whitty, Ind. Eng. Chem. Res. 53 (2014) 2976–2986.
[12] B.M. Corbella, L. de Diego, F. García-Labiano, J. Adánez, J.M. Palacios, Energy Fuels 20 (2006) 148–154.
[13] B. Corbella, L. de Diego, F. Garcia, Energy Fuels 19 (2005) 433–441.
[14] A. Abad, J. Adánez, F. García-Labiano, L.F. de Diego, P. Gayán, Combust. Flame 157 (2010) 602–615.
[15] M. Arjmand, M. Keller, H. Leion, T. Mattisson, A. Lyngfelt, Energy Fuels 26 (2012) 6528–6539.
[16] M. Arjmand, A. Azad, H. Leion, A. Lyngfelt, T. Mattisson, Energy Fuels 25 (2011) 5493–5502.
[17] M.K. Chandel, A. Hoteit, A. Delebarre, Fuel 88 (2009) 898–908.
[18] L.F. de Diego, F. García-Labiano, P. Gayán, J. Celaya, J.M. Palacios, J. Adánez, Fuel 86 (2007) 1036–1045.
[19] A. Abad, I. Adánez-Rubio, P. Gayán, F. García-Labiano, L.F. de Diego, J. Adánez, Int. J. Greenh. Gas Control. 6 (2012) 189–200.
[20] Y. Wen, Z. Li, L. Xu, N. Cai, Energy Fuels 26 (2012) 3919–3927.
[21] Y. Zhang, E. Doroodchi, B. Moghtaderi, Appl. Energy 113 (2014) 1916–1923.
[22] Q. Zafar, T. Mattisson, Energy Fuels 20 (2006) 34–44.
[23] Q. Zafar, T. Mattisson, Ind. Eng. Chem. Res. 2 (2005) 3485–3496.
[24] B. Moghtaderi, H. Song, Energy Fuels 24 (2010) 5359–5368.
[25] S.Y. Chuang, J.S. Dennis, A.N. Hayhurst, S.A. Scott, Chem. Eng. Res. Des. 89 (2011) 1511–1523.
[26] S.Y. Chuang, J.S. Dennis, A.N. Hayhurst, S.A. Scott, Proc. Combust. Inst. 32 (2009) 2633–2640.
[27] S.Y. Chuang, J.S. Dennis, A.N. Hayhurst, S.A. Scott, Energy Fuels 24 (2010) 3917–3927.
[28] E.A. Goldstein, R.E. Mitchell, Proc. Combust. Inst. 33 (2011) 2803–2810.
[29] S.R. Son, K.S. Go, S.D. Kim, Ind. Eng. Chem. Res. 48 (2009) 380–387.
[30] E. Monazam, R. Siriwardane, R. Breault, Energy Fuels 26 (2012) 2779–2785.
[31] I. Iliuta, R. Tahoces, G.S. Patience, S. Rifflart, F. Luck, AIChE J. 56 (2010) 1063–1079.
[32] Z. Zhou, L. Han, G.M. Bollas, Chem. Eng. J. 233 (2013) 331–348.
[33] A. Cabello, P. Gayán, F. García-Labiano, L.F. de Diego, A. Abad, M.T. Izquierdo, et al., Appl. Catal. B: Environ. 147 (2014) 980–987.
[34] M. Ortiz, L.F. de Diego, A. Abad, F. García-Labiano, P. Gayán, J. Adánez, Energy Fuels 26 (2012) 791–800.
[35] I. Adánez-Rubio, P. Gayán, A. Abad, F. García-Labiano, L.F. de Diego, J. Adánez, Chem. Eng. J. 256 (2014) 69–84.
[36] L. Han, Z. Zhou, G.M. Bollas, Chem. Eng. Sci. 104 (2013) 233–249.
[37] L. Han, Z. Zhou, G.M. Bollas, Chem. Eng. Sci. 113 (2014) 116–128.
[38] Z. Zhou, L. Han, G.M. Bollas, Aerosol Air Qual. Res. 14 (2014) 559–571.
[39] The Mathworks Inc., Matlab 2013, 2013.
[40] C. Huo, J. Ouyang, H. Yang, Sci. Rep. 4 (2014) 3682.
[41] Z. Zhou, L. Han, G.M. Bollas, Int. J. Hydrog. Energy 39 (2014) 8535–8556.
[42] H. Song, K. Shah, E. Doroodchi, B. Moghtaderi, Energy Fuels 28 (2014) 163–172.
[43] Y. Li, Q. Fu, M. Flytzani-Stephanopoulos, Appl. Catal. B: Environ. 27 (2000) 179–191.
[44] X. Qi, M. Flytzani-Stephanopoulos, Ind. Eng. Chem. Res. 43 (2004) 3055–3062.
[45] G. Jones, J. Jakobsen, S. Shim, J. Kleis, M. Andersson, J. Rossmeisl, et al., J. Catal. 259 (2008) 147–160.
[46] J. Ereña, J. Vicente, A.T. Aguayo, M. Olazar, J. Bilbao, A.G. Gayubo, Appl. Catal. B: Environ. 142–143 (2013) 315–322.
[47] W.K. Lewis, E.R. Gilliland, W.A. Reed, Ind. Eng. Chem. 41 (1949) 1227–1237.
[48] F. Fischer, H. Tropsch, Brennst. Chem. 9 (1928) 39–46.
[49] B.M. Corbella, L. De Diego, F. García, J. Adánez, J.M. Palacios, Energy Fuels 19 (2005) 433–441.
[50] O. Nordness, Z. Zhou, G.M. Bollas, AIChE Annual Meeting, Atlanta, GA, 2014.
[51] L.F. de Diego, P. Gayán, F. García-Labiano, J. Celaya, A. Abad, J. Adánez, Energy Fuels 19 (2005) 1850–1856.

[52] E. Monazam, R. Breault, R. Siriwardane, Energy Fuels 26 (2012) 6576–6583.
[53] Y. Choi, H.G. Stenger, J. Power Sources 124 (2003) 432–439.
[54] G.F. Froment, K.B. Bischoff, J. De Wilde, Chemical Reactor Analysis and Design, 3rd ed., John Wiley & Sons, Inc., New York, 2011.
[55] T. El Solh, K. Jarosch, H. de Lasa, Ind. Eng. Chem. Res. 42 (2003) 2507–2515.
[56] J.H. Edwards, A.M. Maitra, Fuel Process. Technol. 42 (1995) 269–289.
[57] R. Pereñiguez, V.M. Gonzalez-delaCruz, A. Caballero, J.P. Holgado, Appl. Catal. B: Environ. 123–124 (2012) 324–332.
[58] C. Shi, P. Zhang, Appl. Catal. B: Environ. 115–116 (2012) 190–200.
[59] J.W. Veldsink, G.F. Versteeg, W.P.M. van Swaaij, Chem. Eng. J. 57 (1995) 273–283.
[60] J.L. Ayastuy, A. Gurbani, P. Gonza, M.A. Gutie, Ind. Eng. Chem. Res. 45 (2010) 5633–5641.
[61] G. Avgouropoulos, T. Ioannides, Chem. Eng. J. 176–177 (2011) 14–21.
[62] Z. Zhou, L. Han, G.M. Bollas, Ind. Eng. Chem. Res. (2014) (submitted for publication).
[63] E. Jerndal, T. Mattisson, I. Thijs, F. Snijkers, A. Lyngfelt, Int. J. Greenh. Gas Control. 4 (2010) 23–35.